Cell, Vol. 113, 789–801, June 13, 2003, Copyright ©2003 by Cell Press

Study of the Structural Dynamics of the *E. coli* 70S Ribosome Using Real-Space Refinement

Haixiao Gao,[1,7] Jayati Sengupta,[2,7] Mikel Valle,[1] Andrei Korostelev,[4] Narayanan Eswar,[5] Scott M. Stagg,[6] Patrick Van Roey,[2] Rajendra K. Agrawal,[2,3] Stephen C. Harvey,[6] Andrej Sali,[5] Michael S. Chapman,[4] and Joachim Frank[1,2,3,*]

[1]Howard Hughes Medical Institute
Health Research, Inc.
[2]Wadsworth Center
Empire State Plaza
Albany, New York 12201
[3]Department of Biomedical Sciences
State University of New York at Albany
Empire State Plaza
Albany, New York 12201
[4]Kasha Laboratory
Institute of Molecular Biophysics
and Department of Chemistry and Biochemistry
Florida State University
Tallahassee, Florida 32306
[5]Departments of Biopharmaceutical Sciences and Pharmaceutical Chemistry
and California Institute for Quantitative Biomedical Research
University of California, San Francisco
San Francisco, California 94143
[6]School of Biology
Georgia Institute of Technology
Atlanta, Georgia 30332

Summary

Cryo-EM density maps showing the 70S ribosome of *E. coli* in two different functional states related by a ratchet-like motion were analyzed using real-space refinement. Comparison of the two resulting atomic models shows that the ribosome changes from a compact structure to a looser one, coupled with the rearrangement of many of the proteins. Furthermore, in contrast to the unchanged inter-subunit bridges formed wholly by RNA, the bridges involving proteins undergo large conformational changes following the ratchet-like motion, suggesting an important role of ribosomal proteins in facilitating the dynamics of translation.

Introduction

The ribosome is a highly organized dynamical macromolecule responsible for protein biosynthesis. The dynamic features can be captured by trapping functionally meaningful states and imaging the structure by cryo-electron microscopy (cryo-EM). A recent cryo-EM study of the ribosome (Frank and Agrawal, 2000) found a large conformational reorganization during the elongation cycle of protein synthesis. Following the binding of elongation factor G (EF-G), the small and large subunits undergo a relative ratchet-like motion, accompanied by many local conformational changes during tRNA and mRNA translocation. The question raised by these findings is the nature of the molecular mechanisms underlying the inter-subunit motion. Because of the limited resolution of the cryo-EM maps, currently in the range of 10 Å, the link between the observed global movement of the subunits and their local molecular reorganization is still unknown.

Recently, several atomic structures of ribosomal subunits from the archaean *Haloarcula marismortui* and the bacteria *Thermus thermophilus* and *Deinococcus radiodurans* have been determined by X-ray crystallography at resolutions around 2–3 Å (Ban et al., 2000; Wimberly et al., 2000; Schluenzen et al., 2000; Ogle et al., 2001; Harms et al., 2001). With the aid of the atomic structures of the *T. thermophilus* 30S and *H. marismortui* 50S subunits, a model for the RNA and protein backbone of *T. thermophilus* 70S ribosome was subsequently constructed based on a 5.5 Å X-ray map (Yusupov et al., 2001). The availability of these atomic crystal structures makes it possible to further investigate the ribosomal dynamics by combining structural data from both cryo-EM and X-ray crystallography.

Methods of interpretation of cryo-EM maps of large complexes employing docking and fitting of X-ray structures have received much attention recently (Volkmann and Hanein, 1999; Roseman, 2000; Rossmann, 2000; Wriggers and Birmanns, 2001). In the absence of crystal structures showing the macromolecular complex in different dynamic states, docking techniques still make it possible to construct approximate atomic models. In the present work, a stereochemically restrained real-space refinement technique (Tronrud et al., 1987; Chapman, 1995; Chen et al., 2001) was employed for docking the atomic structures of the 70S ribosome components, including comparative models of proteins, rRNA and tRNA, into the experimental density maps representing different functional states that were obtained by cryo-EM and single-particle reconstruction (Frank, 1996).

Our aim in this work was to understand the local molecular reorganization underlying the "ratchet-like" inter-subunit motion, which is triggered by the binding of EF-G in the presence of a nonhydrolyzable GTP analog ("EF-G·GTP bound state"). The two states that were analyzed are an initiation-like state, with tRNA at the P site, and the EF-G·GTP bound state. These states are not consecutive, but are separated by states associated with decoding and accommodation. Nevertheless, there are indications that the initiation-like complex has a similar conformation as the ribosome prior to EF-G binding. Real-space refinement was used to build atomic resolution models based on the cryo-EM maps of these two states. Since most of the cryo-EM studies and biochemical observations so far were made with the *E. coli* 70S ribosome for which no atomic structure is available, the *E. coli* ribosomal RNA structure was modeled from the crystal structures of the *T. thermophilus* 30S (Ogle et al., 2001) and *H. marismortui* 50S subunits (Ban et al.,

*Correspondence: joachim@wadsworth.org
[7]These authors contributed equally to this work.

2000), accounting for the species-dependent variations. In addition, ribosomal proteins from *E. coli* were modeled by comparative protein structure prediction based on their sequence similarity to structurally defined homologs from other species (Martí-Renom et al., 2000).

The building of the models was guided mainly by the experimental density maps obtained from cryo-EM. The atomic structures of RNA and protein were cut into pieces of presumed stability and fitted into the experimental density map while observing stereo-chemical constraints. In the light of the atomic models that represent the two states of the ratchet-like movement, we analyzed the local molecular conformational rearrangements of RNA and proteins. Our study shows that the most extensive molecular rearrangements are seen in the ribosomal proteins. Specifically, proteins S13, S19, L2, L5, and L14 are seen to be involved in the control of the relative movement of the subunits through their inter-subunit bridges.

Results

Structural Modeling

The three-dimensional cryo-EM density maps of *Escherichia coli* 70S ribosome complexes studied by real-space refinement are: (1) an 11.5 Å map (Gabashvili et al., 2000) of the initiation-like complex with fMet-tRNA$_f^{Met}$ at the P site (Malhotra et al., 1998) and (2) a 12.3 Å map of the EF-G·GTP bound complex, i.e., a ribosome bound with EF-G in the presence of a nonhydrolyzable GTP analog. This latter map is a higher-resolution version (M.V., unpublished data) of the earlier 18 Å map of this complex (Agrawal et al., 1999a; Frank and Agrawal, 2000).

The *E. coli* 70S ribosome consists of two subunits, which are designated as the 30S subunit, comprising 16S rRNA (1542 nucleotides) and 21 proteins, and the 50S subunit, comprising 23S rRNA (2904 nucleotides), 5S rRNA (120 nucleotides), and 36 proteins. The models of *E. coli* 23S rRNA and 5S rRNA were generated from the crystal structure of *H. marismortui* (PDB code 1FFK), while the model of *E. coli* 16S rRNA was generated from the crystal structure of *T. thermophilus* (PDB code 1IBL). The molecular modeling package Insight II (Accelrys Inc.) was used to model the sequences of the ribosomal RNA of the *E. coli* based on the crystal structures and also to model the helices 38, 43, 44, 69, and 76 of 23S rRNA, which were unresolved in the *H. marismortui* 50S structure.

All of the *E. coli* ribosomal protein structure models were calculated by ModPipe, a completely automated large-scale protein structure-modeling pipeline (Sanchez and Sali, 1998; Pieper et al., 2002). The crystal structures of the proteins from the small subunit of *T. thermophilus* (PDB code 1FJG) were chosen as the structural templates to model 19 proteins of the 30S small subunit (S2–S20) of *E. coli*. For proteins of the 50S subunit, 29 out of all the 36 *E. coli* proteins were modeled based on the 50S crystal structure of *H. marismortui* (PDB code 1JJ2; L2, L3, L4, L6, L14, L15, L16, L18, L24, L29, and L30), the 50S crystal structure of *D. radiodurans* (1LNR; L5, L11, L13, L17, L19, L20, L21, L22, L23, L27, L31, L32, L33, L34, L35, and L36), and the 70S crystal structure of *T. thermophilus* (1GIY; L9, L25), respectively. Model building began by generating a multiple sequence profile for each one of the *E. coli* sequences and the potential template structures. Next, the sequence-structure matches for model building were obtained by aligning the profile of each *E. coli* sequence against the sequences of the template structures using PSI-Blast (Altschul et al., 1997), and also by aligning the profiles of the template structures against the *E. coli* sequences using IMPALA (Schaffer et al., 1999). Alignments that had a significant e-value and covered distinct regions of the *E. coli* sequences were then chosen for modeling. Models were calculated for each one of the sequence-structure matches using MODELLER (Sali and Blundell, 1993). The resulting models were then evaluated using statistical potentials of model compactness, the sequence identity of the sequence-structure match, and energy z-scores to assess the quality of the model. The final selection of models for docking was determined from the e-value of the alignment, the quality of the final model, and the quality of the template structure. The characteristics of each protein model (sequence identity, e-value of the alignment, and model score) are listed in the Supplemental Data available at http://www.cell.com/cgi/content/full/113/6/789/DC1. Proteins L1 and L7/L12 were not included because their corresponding cryo-EM densities are not well defined, or are fragmented due to their high flexibilities. Additionally, several proteins, including L21, L32 and L35 in the 50S subunit, were excluded from the final model as the qualities of their homology models are very low. L34 was excluded because its features cannot be distinguished in the cryo-EM maps.

The starting model was built by manually docking the RNA and protein structures, each as a rigid body, into the cryo-EM density maps using the interactive program O (Jones et al., 1991). The initial position of each RNA structure and protein was taken from the position of the corresponding crystal structure template.

The program RSRef (Chapman, 1995), a real-space refinement module for the TNT program (Tronrud et al., 1987), was employed for automatically and simultaneously refining both the stereochemistry and the fit of the atomic structures to the density map. Since the resolutions of the experimental density maps are not suitable for refinement of independent atoms, a multi-rigid-body refinement was employed. The progressive cutting into smaller rigid units of RNA and protein was based on the statistics of both the stereochemistry and the fit to the density map in each round of refinement. Initially, the RNA was cut into domains and each protein molecule was treated as a single rigid body. Real-space refinement produced significant overall improvement, but a large number of the poor van der Waals contacts could not be resolved, and some local areas, such as the spur and beak regions of the 30S subunit, showed substantial conflicts with the density map. Inspection showed that the regions of poor fit to the experimental density map and an excessive number of close contacts were predominantly regions with known flexibility, species-dependent structural variations, or experimental evidence of disorder. The RNA and proteins were therefore further cut into components/blocks in those poorly fitted regions. The integrity of the double-helical regions

was maintained with cuts only applied in single-stranded and loop regions. Most of the proteins were retained as single rigid units. Exceptions included S2, S7, S13 in the 30S subunit and L2, L3, L5, L6, L9, L11, L18, and L24 in the 50S subunit, which were cut into their major domains. In addition, for some proteins, namely S7, S9, S11, S12, L3, L4, L15, L17, L20, L23, L27, and L32, unstructured flexible extensions that are attached to RNA were removed to avoid severe van der Waals overlap. Typically, proteins moved by up to 10 Å during the refinement. The final assignment of RNA rigid bodies is shown in Figure 1, including 43 pieces of 16S rRNA, 62 pieces of 23S rRNA, and 4 pieces of 5S rRNA.

The 70S Ribosomal Models in Two States

An *E. coli* 70S ribosome model for the initiation-like state was generated by fitting a total of 165 fragments of RNA and proteins into the 11.5 Å EM density map using the real-space refinement algorithm. As shown in Figure 2, all of the 44 proteins, 23S rRNA, 16S rRNA, and 5S rRNA fit very well into the density map. The overall appearance of the model is very similar to the crystal structures from other species. A total of 19 proteins in the 30S subunit were fitted, most of which are near the solvent surface, except for S12, S13, and S19. In the 50S subunit, among all the 25 fitted proteins, L2, L5, L14, and L19 are located on the inter-subunit surface, forming bridges with the 30S subunit.

Similarly, a model of the *E. coli* 70S ribosome in the EF-G·GTP bound state was built from the same set of coordinates used to model the ribosome in the initiation-like state. Since protein S2 is fragmented in the cryo-EM map of the EF-G·GTP bound state and part of the mass of protein L9 is missing, a total of 162 rigid fragments of RNA and proteins were subjected to the refinement in this case.

For a more detailed appraisal of the two fitted structures of the initiation-like and the EF-G·GTP bound state, Figure 3 depicts the fittings in the maps of the 30S subunit and the 50S subunit separately. In the 30S subunit in both states (Figures 3A and 3B), the whole 16S rRNA is seen to be satisfactorily placed in the experimental maps, especially in the regions of the spur, beak, and shoulder, which are known to be the most different from the crystal structures of the 30S subunit (Ogle et al., 2001). For many of the proteins that are located near the surface and have distinct shapes, such as S2, S6, S11, and S15, the fitting was particularly straightforward and reliable. Similarly, in the case of the 50S subunit (Figures 3C and 3D), the overall models are also in excellent agreement with the density maps.

The quality of the model was assessed with three quantitative indicators: crosscorrelation coefficient, real-space R factor, and number of bad van der Waals contacts. Shown in Table 1 is a summary of the fitting statistics of the models in the initiation-like and the EF-G·GTP bound states before and after the real-space refinement. As indicated by the correlation coefficient and R factor, the real-space refinement resulted in substantial improvements in the fitting of the density maps, and the numbers of van der Waals overlaps are also reduced to a modest range (1000–2000, compared to a total 120,000 atoms). Furthermore, to assess the local fitting quality, the correlation coefficients were computed for each of the ribosomal RNA fragments and proteins (Supplemental Data available at http://www.cell.com/cgi/content/full/113/6/789/DC1).

All three RNA structures (16S rRNA, 23S rRNA, and 5S rRNA) achieved high correlation coefficients in both states: 0.74–0.80 for the initiation-like state and 0.68–0.69 for the EF-G·GTP bound state. For the proteins, with few exceptions, the correlation coefficients of the proteins are above 0.6, indicating satisfactory fitting. Among the small-subunit proteins, the correlation coefficient of S18 was the poorest. Interestingly, S18 is located near S1, which is known to have very weak association with the ribosome (Laughrea and Moore, 1977). As S1 directly interacts with S18 (Sengupta et al., 2001), it is conceivable that the detachment of S1, either partially or fully, might introduce conformational changes that affect S18. In addition, those proteins that show high mobility and undergo significant rearrangement, such as S7, S13, and S19 in the 30S subunit and L2, L9, and L13 in the 50S subunit, usually appear to have lower correlation coefficients compared to less mobile proteins. The lower correlation coefficient can be easily explained as a result of the averaging over different conformations exhibited in the sample.

Inter-Subunit Bridges

The inter-subunit bridges are important for maintaining the overall architecture of the ribosome (Frank et al., 1995a; Cate et al., 1999; Gabashvili et al., 2000), but can also be expected to play a role in the dynamics of translation (Frank and Agrawal, 2000, 2001). An earlier cryo-EM study (Gabashvili et al., 2000) identified a total of 13 inter-subunit connections based on the separation of the EM density map of the 11.5 Å initiation-like complex. Recently, Yusupov and coworkers (2001), using their 5.5 Å crystal structure, identified more than 30 individual inter-subunit interactions spread among 12 bridges in the *T. thermophilus* 70S ribosome.

In our newly generated *E. coli* model in the initiation-like state, all of the earlier identified bridges are interpreted as discrete, sometimes multiple atomic contacts. Table 2 lists the bridges and their constituent components from both subunits in the initiation-like complex, following the nomenclature of Frank and coworkers (1995a) and expanded in subsequent studies (Cate et al., 1999; Gabashvili et al., 2000; Yusupov et al., 2001). For each bridge identified in the *T. thermophilus* ribosome, there exists a counterpart in the *E. coli* structure. Furthermore, many bridges in *E. coli* are virtually identical to the bridges found in the *T. thermophilus*, in terms of their locations and the RNA helices and proteins involved. The high similarity suggests that the inter-subunit bridge regions are highly conserved across species, and that their atomic makeup is essential for function. The same observation was made in a comparison of the inter-subunit bridges between bacterial and yeast ribosomes (Spahn et al., 2001).

More than 80 percent of the bridges in the *E. coli* involve contacts with helices 23, 24 (central domain) and 44 (3′ minor domain) from the 30S subunit side (Figure 4A), and helices 64 and 67–71 (domain IV) from the 50S subunit side (Figure 4B). One of the bridge regions that

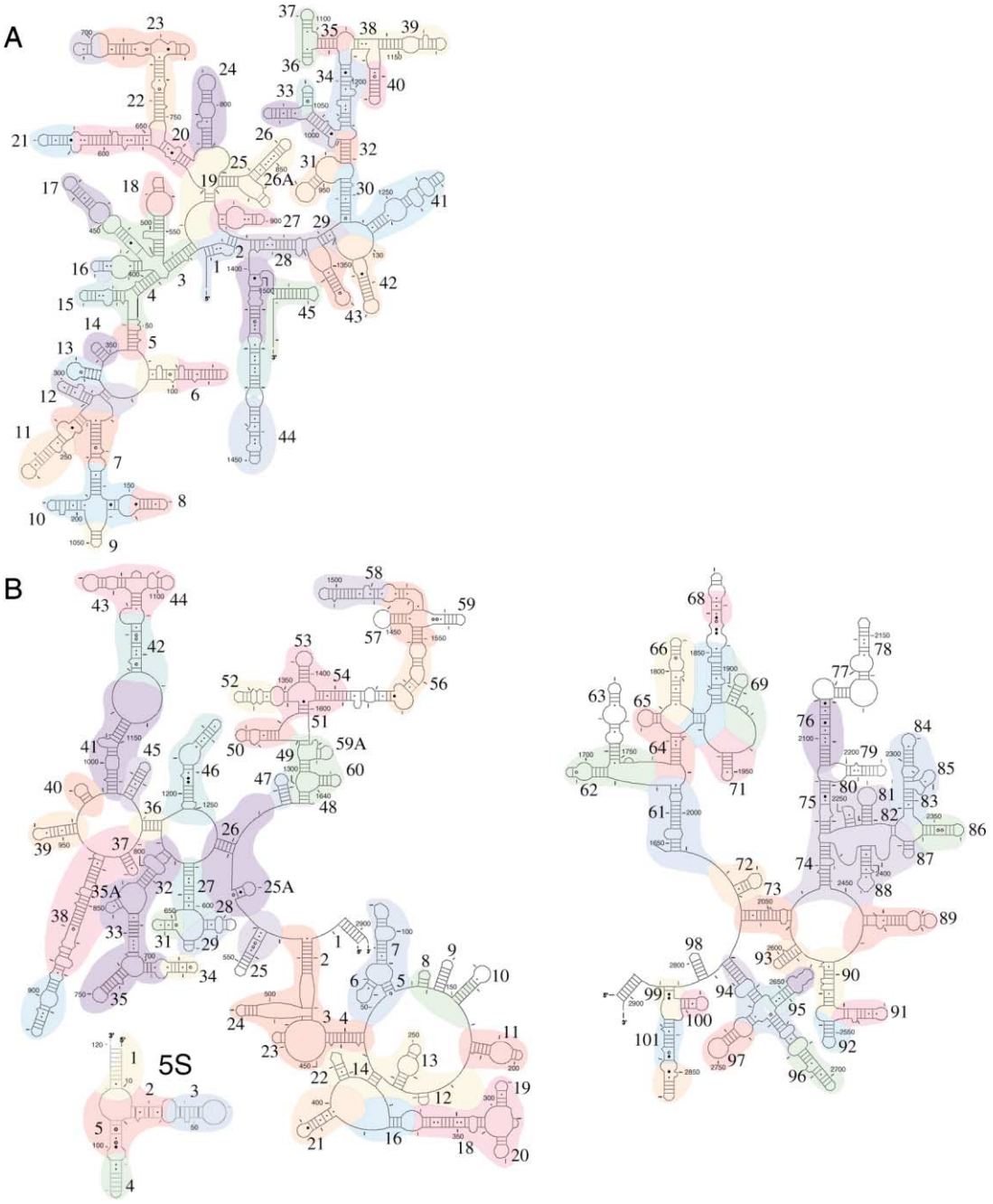

Figure 1. The Rigid Body Assignment of Ribosomal RNA Secondary Structure Elements

The rigid bodies are shaded in different colors on the secondary structure maps of (A) 16S rRNA, and (B) 23S rRNA and 5S rRNA, respectively. Uncolored regions are not included in the model (see details in the Supplemental Data available at http://www.cell.com/cgi/content/full/113/6/789/DC1).

differed between the previous *E. coli* and *T. thermophilus* structures is at the connection between S13 and L5, which is depicted as two distinct bridges, B1b and B1c, in *E. coli,* but only one connection was identified in *T. thermophilus* as B1b. However, inspection of our new model in the initiation-like state indicates that there are no significant differences between *E. coli* and *T. thermophilus* in the S13 residues that participate in this bridge. In addition, several newly identified bridging contacts include protein S19 (B1a) and helix 22 (B7b) of the 30S subunit, protein L19 (B8), and helices 66 (B2c) and 71 (B5) of the 50S subunit.

In order to investigate all the conformational changes in the bridge regions and the underlying mechanism, the bridges in the EF-G·GTP bound complex were also identified (Table 2), based on the fitted model of the 70S ribosome in this state. A comparison of the two sets of bridges in Table 2 indicates that the changes take place

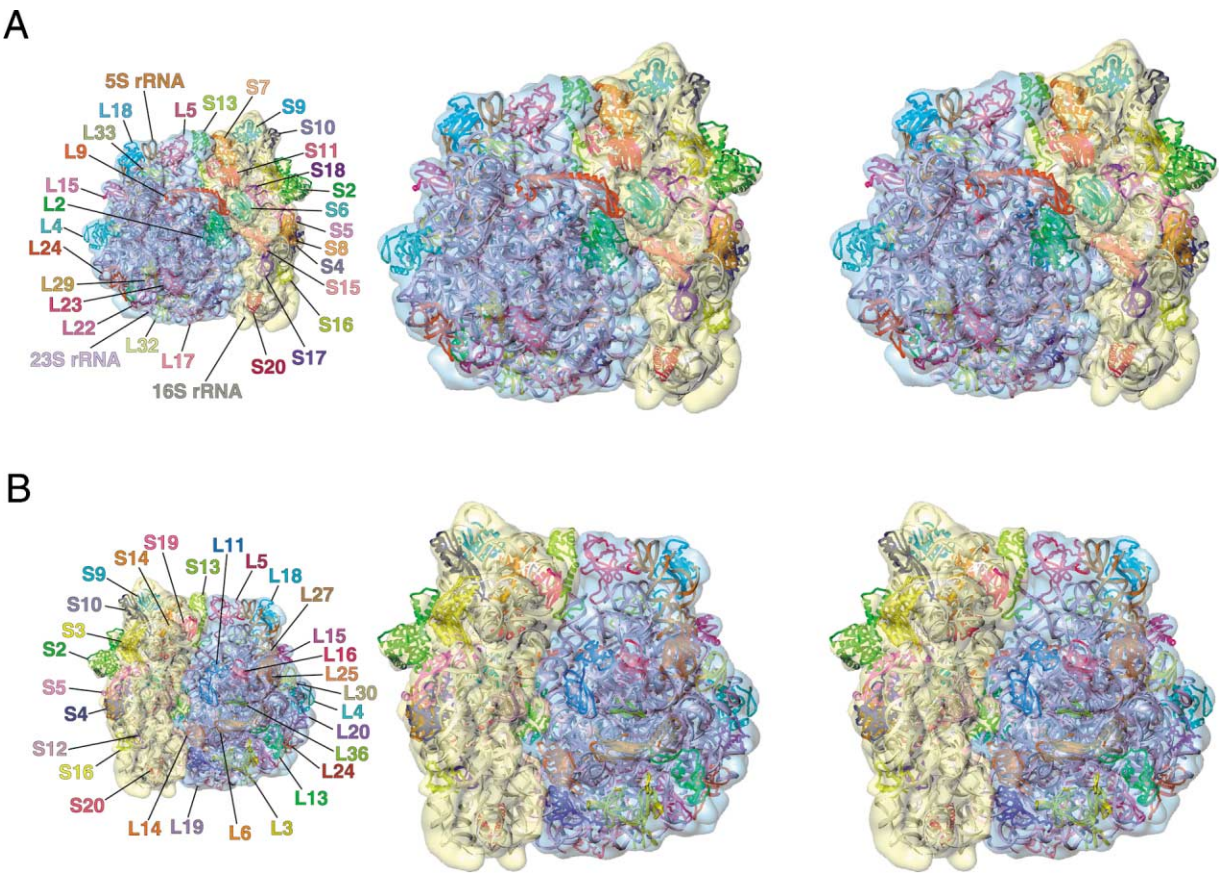

Figure 2. Stereo Views of the Overall Fitting of the Initiation-Like State of the 70S Ribosome Complex

(A) Side view, with the 30S subunit on the right and the 50S subunit on the left.

(B) View obtained by rotating the ribosome by 180° from (A) around an axis running vertical in the image plane. The ribosome is shown by semitransparent contours in yellow (30S) and blue (50S). The models of 16S rRNA (silver), 23S rRNA (purple), 5S rRNA (orange) and proteins (in varied colors) are displayed by Ribbons (Carson, 1991).

mainly in bridges involving protein-protein or protein-RNA interactions as in B1a, B1b, and B7b. B1a and B1b were earlier identified as being strongly affected by the ratchet motion (Frank and Agrawal, 2000). A detailed discussion of these bridges follows later.

Atomic Interpretation of the Ratchet-Like Movement

Superimposition of the experimental density maps of the initiation-like state and the EF-G·GTP bound state immediately reveals the ratchet-like rotation of the 30S subunit relative to the 50S subunit. The observed relative inter-subunit movement is very similar to that from the earlier study (Frank and Agrawal, 2000), except that the overall rotation angle is smaller than previously reported (4° instead of 6.5°). In order to quantitatively analyze the local movement of the ribosomal RNA for each residue of the RNA structure, we calculated its displacement from the initiation-like to the EF-G·GTP bound state on the basis of the two fitted models. We computed a displacement map (Figure 5), in which each residue was assigned a color according to its absolute displacement. Going from the blue to the red regions, the value of the local displacement is increasing, implying an increase in the size of the movement. Overall, the movement range of 16S rRNA is between 0–10 Å (Figure 5A). The large-scale rotation of the 30S subunit is represented mainly by a movement of the head (4°), the shoulder (3°), and spur region (8°). The regions showing largest movements (red areas in Figure 5A) are the head domain of the 16S rRNA, particularly helices 39, 41 and 42, and the spur (helix 6). Interestingly, the mobility of the head has been predicted both from the 16S secondary structure (Yusupov et al., 2001) and from neutron scattering (Serdyuk et al., 1992). The region showing the smallest movements (colored in blue in Figure 5A) contains the geometric center of the rotation comprising helices 2, 7, 14, 19, 21, 26, 27, and 44. Most of this relatively stable 30S subunit region participates in the formation of the centrally located inter-subunit bridges, which anchor it to the 50S subunit. In general, going from the inner region of the 16S RNA to the peripheral region, the displacement of the local structure gradually increases as indicated by the change of the assigned color from blue to yellow and then red.

The overall rotation of the 16S rRNA with respect to the 23S rRNA can be characterized in an orthogonal coordinate system by three rotational angles, around the x-axis (normal to the subunit interface), the y-axis (head to bottom), and the z-axis (shoulder to platform) with the values of 3.3°, 0.5°, and 0.7°, respectively. The

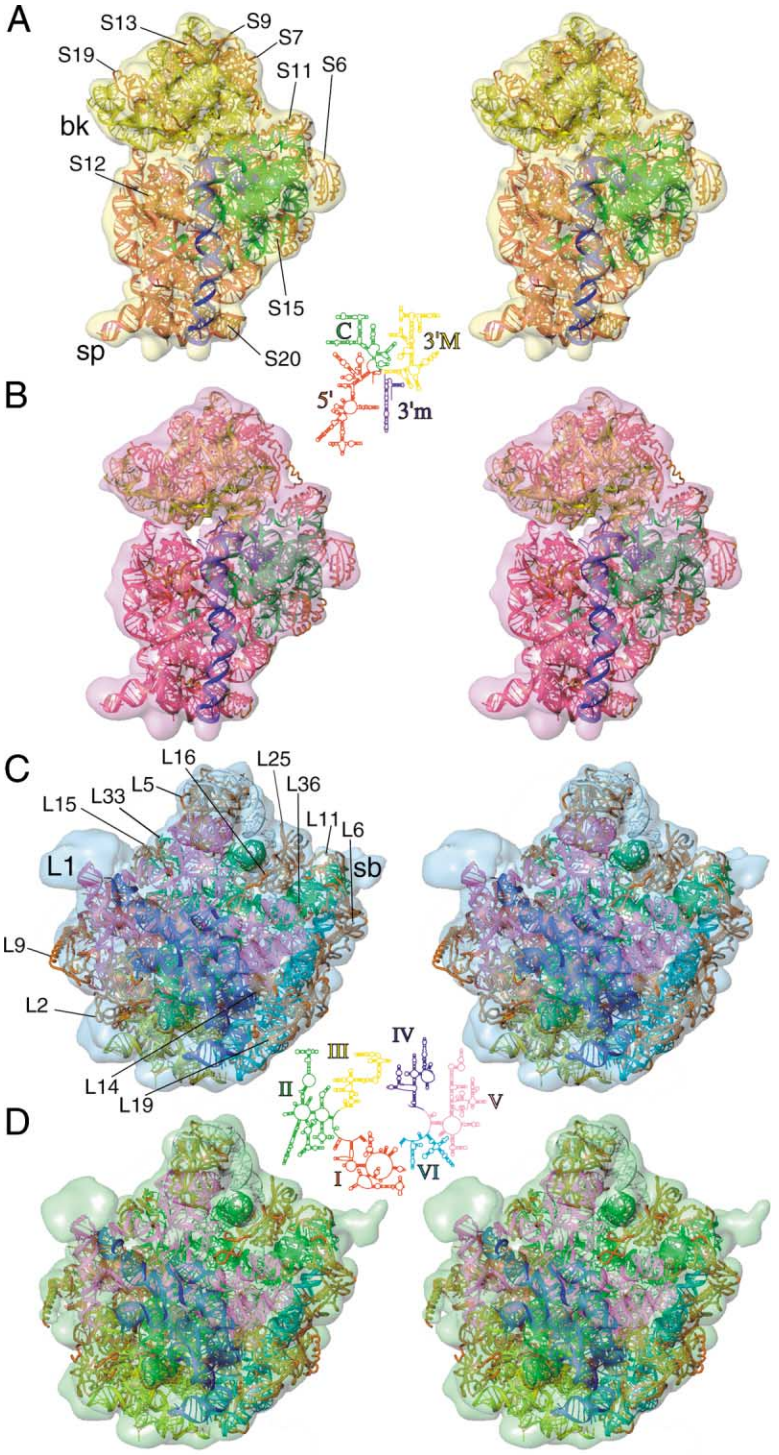

Figure 3. Stereo Views of the Fittings of the Initiation-Like Complex and the EF-G·GTP Bound Complex

The fittings of the initiation-like state complex and the EF-G·GTP bound complex are presented in pairs.

(A and B) Inter-subunit view of the 30S subunit and (C and D) inter-subunit view of the 50S subunit. The density maps are shown as semitransparent contours (30S initiation-like, yellow; 30S EF-G·GTP bound, pink; 50S initiation-like, blue; 50S EF-G·GTP bound, green). The RNA structures are colored according to domains. For 16S rRNA, these are 5′ (red), central (green), 3′ major (yellow) and 3′ minor domain (blue). For 23S rRNA and 5S rRNA, these are domain I (red), II (green), III (yellow), IV (blue), V (pink), VI (cyan) and 5S (silver). All the proteins are in orange. Landmarks: bk, beak; sp, spur; L1, protein L1; sb, L11 stalk base.

30S subunit regions that undergo substantial reorganizations in the course of the ratchet-like movement are located at the mRNA entrance and exit channels, and in the head region that forms the only protein-protein inter-subunit bridge. A comparison between the fitted models of the two states shows that these local rearrangements are mostly related to the movement of proteins.

The path of mRNA in the 30S ribosome was proposed and mapped by cryo-EM (Frank et al., 1995b; Frank et al., 2000) and X-ray crystallography (Yusupova et al., 2001). The mRNA entrance channel is formed mainly by proteins S3, S4, and S5. With protein S3 in the lower region of the head, S4 near the shoulder, and S5 at the top center of the body, these three proteins define a triangular opening between head and shoulder of the 30S subunit. The relative movements between S3, S4, and S5, from the initiation-like state to the EF-G·GTP

Table 1. Fitting Statistics of *E. coli* 70S Ribosome Models in the Two States

	Initiation-Like State	EF-G-GTP Bound State
Map resolution (Å)	11.5	12.3
Initial correlation coefficient	0.53	0.37
Final correlation coefficient	0.71	0.67
Initial R factor	0.29	0.32
Final R factor	0.23	0.24
Initial van der Waals close contacts	>10,000	>10,000
Final van der Waals close contacts	~1900	~1200

bound state (Figure 6A), result in an opening up of the mRNA entrance channel (Frank and Agrawal, 2000). Similarly, the mRNA exit channel, which is located between head and platform, and is surrounded by S7, S11, S18 and helices 23, 24, 28, and 45 of the 16S rRNA, becomes wider in the EF-G·GTP bound state than in the initiation-like state, clearly due to the relative movements between proteins and part of the head region of 16S RNA (Figure 6B). S13, the protein bridging the head of the 30S subunit with the central protuberance of the 50S subunit, stands out among all the proteins of the 30S small subunit by displaying the largest movement. The displacement of the N-terminal region of S13 is about 12 Å between the two states. In the initiation-like state, the C-terminal of S13 is close to the location of the P-site tRNA, connecting with the tip of helix 38 of 23S RNA of the 50S subunit. In the EF-G·GTP bound state, it departs from the previous position by an ~15 Å movement, thereby breaking the connection with the protruding tip of helix 38. Another region that undergoes a large conformational rearrangement comprises S6, S18, and S11, which form a rather compact cluster in the initiation-like state while changing into a looser one in the EF-G·GTP bound state.

S12, the only protein close to the decoding center (Brodersen et al., 2002), is also the only known protein in the 30S subunit that interacts with EF-G (Agrawal et al., 1998). S12 is therefore expected to have an important role during translocation. From the initiation-like to the EF-G·GTP bound state, S12 is observed to undergo a rotation by about 19 degrees toward the inter-subunit space, possibly positioning the protein such that it is able to contact EF-G. Interestingly, two independent

Table 2. Bridges between the 30S and 50S Ribosomal Subunits[a]

Bridge	Type	30S Component	RNA or Protein Positions	50S Component	RNA or Protein Positions	*E.coli* Nomenclature[b]
B1a	p-R	S13	102–115	H38	881–883[c]	(B1a)
	p-R	S19	83–84	H38	884–885,891–892	
B1b	p-p	S13	2–8	L5	110–114,130–136	(B1c)
	p-p	S13	56–67	L5	110–114,130–136	(B1b)
B2a	R-R	h44	1409–1410,1495–1496	H69	1912–1913	(B2a)
B2b	R-R	h24	783–786,791–792	H67	1836–1838,	(B2b)
				H69	1922–1923,1928–1929	
		h45	1514–1516	H67,H71	1833–1834,1932–1933	
B2c	R-R	h24	770–774	H66,H67	1793–1794,1830–1833	(B2c)
		h27	900–901	H67	1832	
B3	R-R	h44	1483–1486	H71	1948–1949,1960–1962	(B3)
B4	R-R	h20	762	H34	715–716	(B4)
	p-R	S15	59–63,86–87	H34	714–716	
B5	R-R	h44	1418–1419	H64	1718–1719	(B3a,b)
	R-R	h44	1420–1421	H71	1950–1951	
	R-p	h44	1421–1423	L14	45–50	
	R-R	h44	1473–1476	H62	1689–1690,1702–1703	
				H64	1988–1989	
B6	R-R	h44	1429–1431	H62	1704–1705	
	R-p	h44	1432–1433	L19	107–110	
	R-p	h44	1463–1465	L19	108–113	
B7a	R-R	h23	698–699,701–703	H68	1847–1848,1896–1897	(B2d)
B7b	R-p	h23	712–714	L2	240–244	(B2e)
	R-p	h24	773–776	L2	226–227,247–251	
	R-p	h22	669–671	L2	235–238	
B8	R-p	h14	339–340,345–346	L14	13,97–98	(B6)
	R-p	h14	345–346	L19	39–43	

R, RNA; p, protein; h, helices in 30S; H, helices in 50S.

[a] In the EF-G.GTP bound state, B1a and B7b are broken, and resides involved in B1b change into:

	p-p	S13	17–22	L5	141–145	
	p-p	S13	64–70	L5	110–113,132–135	

[b] Gabashvili et al, 2000.

[c] The missing residues 886–890 from the model are very likely involved in B1a.

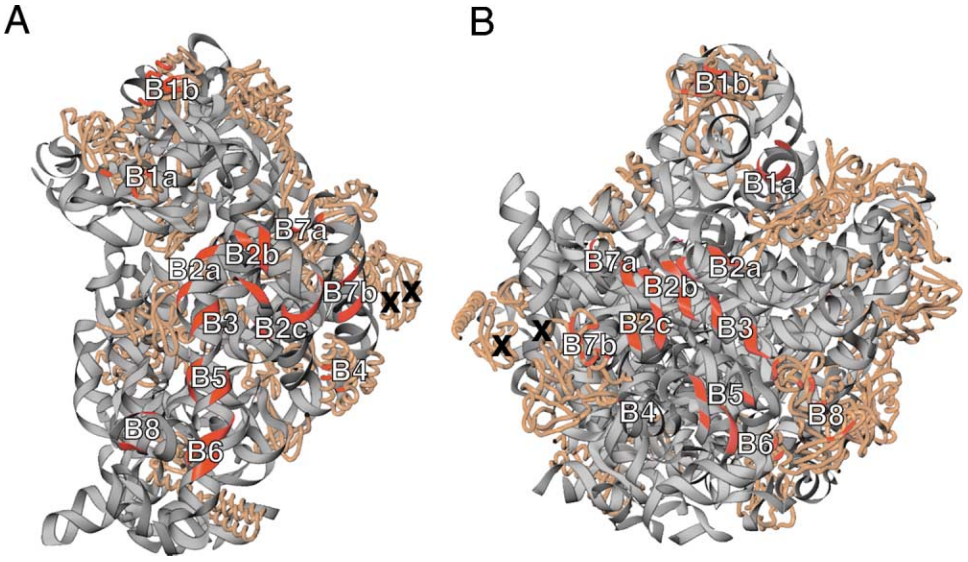

Figure 4. Inter-Subunit Bridges of *E. coli* 70S Ribosome in the Initiation-Like State

Inter-subunit view of 30S subunit (A) and 50S subunit (B), with the bridges numbered and shaded in red. X marks regions of close contact between proteins S6 and L2/L9. RNA and proteins are colored in gray and golden, respectively.

cryo-EM studies of the *E. coli* 70S ribosome bound aa-tRNA·EF-Tu·GTP complex (Valle et al., 2002; Stark et al., 2002) both reported a significant movement of S12.

All the proteins of the 30S subunit are found in both the initiation-like and EF-G·GTP bound states, except for S2. The mass attributable to S2 was partially missing from the EF-G·GTP bound state but fully presented in the initiation-like state. S2 is located at the hinge between the head and body of the 30S subunit (Brodersen et al., 2002), two regions that undergo a large relative movement. This displacement suggests that the partial absence of S2 in the map of the EF-G·GTP bound state could be associated with the local instability of the region to which it is attached.

In the case of the 50S subunit, the superimposition of the two EM density maps indicates an absence of large-scale movements. However, many local movements can be deduced from the comparison of the fitted models in the two states. As shown in Figure 5B, most of the regions in 23S rRNA and 5S rRNA appear to be less mobile than average, in contrast to the behavior of 16S rRNA, with movements generally less than 3 Å, with the exception of 5S rRNA and helices 43, 44, 76, and 86 of 23S rRNA.

Helix 76 of domain V of the 23S rRNA belongs to the so-called L1 stalk along with helices 77, 78, and protein L1. The mobility of the L1 stalk has been inferred from its different locations in different cryo-EM (Gomez-Lorenzo et al., 2000; Valle et al., submitted) and crystal structures (Harms et al., 2001; Yusupov et al., 2001). It

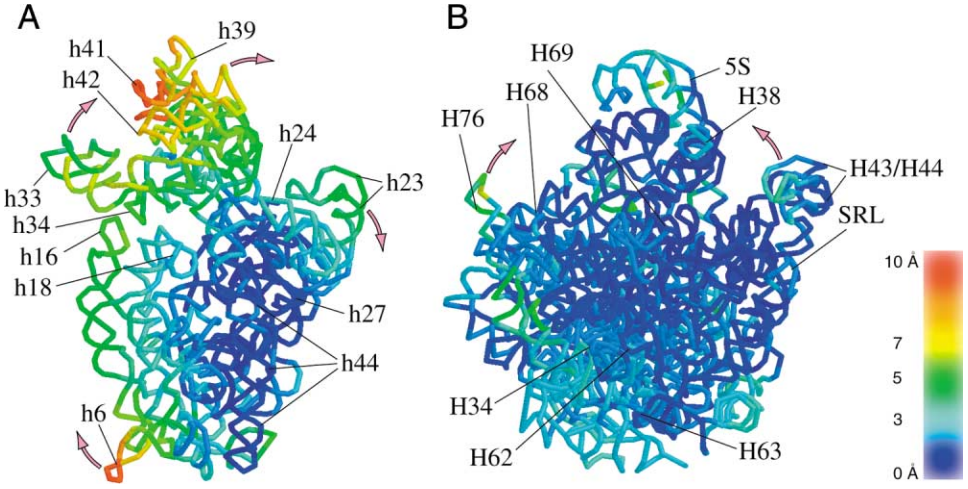

Figure 5. Displacement of RNA Structure between the Initiation-Like and the EF-G·GTP Bound States

(A) 16S rRNA, (B) 23S, and 5S rRNA. Each residue was assigned a certain color according to its displacement calculated from the models. The color bar represents the displacement value assigned to each color.

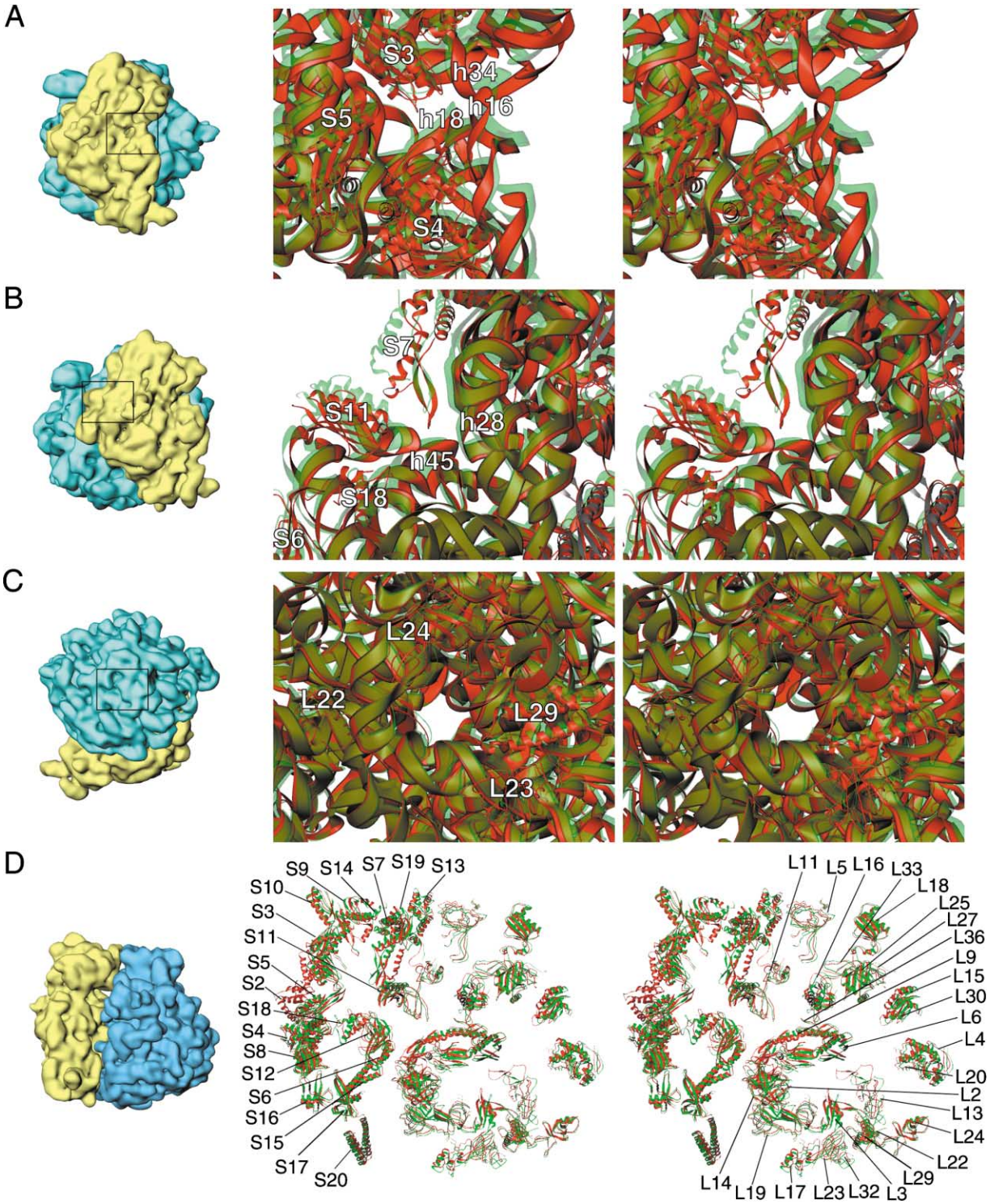

Figure 6. Stereo Views of the Protein Conformational Changes between the Initiation-Like and the EF-G·GTP Bound States

The proteins in the initiation-like and the EF-G·GTP bound states are colored in red and green, respectively.

(A) mRNA entrance channel.

(B) mRNA exit channel.

(C) Polypeptide exit tunnel.

(D) 70S proteins.

has been proposed to facilitate the release of the E-site tRNA (Agrawal et al., 1999b; Gomez-Lorenzo et al., 2000; Yusupov et al., 2001; Harms et al., 2001) and to be actively involved in the translocational movement of tRNA from the P site to the E site (Valle et al., submitted). Despite the absence of helices 77, 78, and protein L1 from our current model, a comparison of the positions of helix 76 in the two states indicates a pronounced movement as it swings by 15° toward the central protuberance (CP), in effect blocking the inter-subunit space, when going from the initiation-like to the EF-G·GTP bound state.

Forming the RNA part of the L7/L12 stalk base, helices 43 and 44 constitute another flexible region in the 50S subunit, as observed from both X-ray crystallography (Harms et al., 2001) and a cryo-EM study of EF-G-dependent translocation (Agrawal et al., 2001). From the initiation-like to the EF-G·GTP bound state, there is a movement of helices 43 and 44 toward helix 38 coupled to a 3–4 Å movement of the L11 N-terminal domain toward the G domain of EF-G (Agrawal et al., 2001). The C-terminal domain of L11, being tightly attached to helices 43 and 44, rides along with them. These movements are associated with the interaction of this region with domain V of EF-G in the EF-G·GTP bound state. In addition, the protruding tip of helix 38 shows significant movements between the two states, accompanied by the changes of the inter-subunit bridge B1a.

In the case of the 50S subunit proteins, from the initiation-like to the EF-G·GTP bound state, many proteins near the solvent surface follow an outward movement, especially those proteins that lie close to the different branches of the polypeptide exit tunnel (Frank et al., 1995b; Nissen et al., 2000; Gabashvili et al., 2001), such as L22, L23, L24, and L29 (Figure 6C).

One intriguing phenomenon emerging from this study concerns the 50S subunit proteins close to the subunit interface, in particular L5, L2, and L14. From the initiation-like to the EF-G·GTP bound state, these proteins undergo significant local movements and rearrangements. L5 is the only protein in the 50S subunit that forms a protein-protein bridge (B1b), with protein S13 of the 30S subunit. The overall movement of L5 between the initiation-like and the EF-G·GTP bound states can be characterized as a 13° rotation, apparently related to the large movement of protein S13 as the subunits rotate relative to each other. This large movement of L5 thus helps to maintain the connection between L5 and S13. Similarly, proteins L2 and L14, which are involved in B5, B7b, and B8, show high mobility. As discussed shortly, the movements of these proteins can be correlated with the crucial dynamic role of the inter-subunit bridges during translocation.

Discussion

Following the first report of the ratchet-like movement of 70S ribosome during EF-G-dependent translocation (Frank and Agrawal, 2000), similar motions have been observed in other functional ribosomal complexes (Valle et al., submitted; Spahn et al., submitted). A recent normal mode analysis of the 70S crystal structure of *T. thermophilus* (Tama et al., submitted) indicated a similar inter-subunit movement, in striking agreement with that observed experimentally, implying that this motion might be an intrinsic behavior that follows from the overall shape of the ribosome.

Due to the limitations in resolution and quality of the experimental density maps, and the fact that no structure data are available for some proteins and RNA components, the real-space refinement protocol was chosen as the best approach for exploiting the currently available structural information to the maximum extent. RSRef, the real-space refinement method selected to build models of the ribosome in different functional states, produced satisfactory results as the new models account for the experimental observations. To give an example for the pronounced sensitivity of the quality indicators (local correlation coefficient and R factor) to small positional changes, a 2 Å shift reduces the local correlation coefficient from 0.73 to 0.66 and degrades the R factor from 0.24 to 0.26, for a typical protein (L6; see Supplemental Data available at http://www.cell.com/cgi/content/full/113/6/789/DC1). As a rule, the fitting quality of the initiation-like state exceeds that of the EF-G·GTP bound state, evidently since the EF-G·GTP bound state is characterized by a looser, less stable conformation.

During the preparation of this paper, a homology model of the *E. coli* 30S ribosomal subunit based on the crystal structure of the *T. thermophilus* 30S ribosomal subunit was published (Tung et al., 2002). The crosscorrelation coefficient between the 16S rRNA of this homology model and the 11.5 Å EM density map is 0.56. Our real-space-refined model for the initiation-like state gives a substantially better value of 0.80. This discrepancy is most likely due to the lack of a restraint to the cryo-EM data in the modeling of Tung and coworkers.

The Dynamics of the Inter-Subunit Bridges

Based on examination of the inter-subunit bridges identified in the two states, the behavior of the bridges subjected to the ratchet-like inter-subunit movement can be classified into two types: (1) bridges that are rather stable and almost unchanged and (2) bridges whose molecular contacts are changed or broken as they absorb large displacements far away from the geometrical axis of rotation. The first type includes all the RNA-RNA bridges, such as B2a-c, B3, B5, and B7a. As the large-scale relative motion between the 30S and 50S subunit takes place, these bridges remain stable and show only a small ($<$3Å) local rearrangement. In contrast, most of the bridges involving proteins behave in quite a different way. A case in point is B1b, the only bridge formed by proteins, connecting S13 and L5. As both S13 and L5 undergo large movements during the large-scale inter-subunit movement, their residues involved in the B1b contacts apparently switch from one set to another (Table 2), likely playing the important role of regulating and stabilizing the ribosome as it goes from one state to the other. Other examples are the bridges that are well connected in the initiation-like state and subsequently broken in the EF-G·GTP bound state, including B1a and B7b. B1a is located between S13, S19 of the 30S subunit and helix 38 of the 50S subunit, and B7b is between helices 22–24 of the 30S subunit and L2 of the 50S

subunit. The two bridges are both formed by RNA-protein interactions, and the disruptions are due to the protein side of the bridges undergoing large movements, while the RNA side is quite static. Interestingly, the two bridges (B5 and B8) that involve protein L14 show no significant change in terms both of the connection distance and the participating residues, although L14 itself undergoes a 14° rotation. Closer inspection reveals that the movement of the bridge is small because the bridge interaction region on protein L14 is close to the protein's rotation center.

Our results show that the inter-subunit RNA-RNA bridges in the central part of the 70S ribosome remain virtually unchanged, evidently maintaining the stability of the 70S assembly while allowing the functionally important ratchet motion to occur in response to EF-G·GTP binding. It is likely that due to the stability of the subunit connection formed by the central bridges, the ratchet motion imposes a strain on the RNA framework of the subunits that forces it to return to the "ground state" of the control.

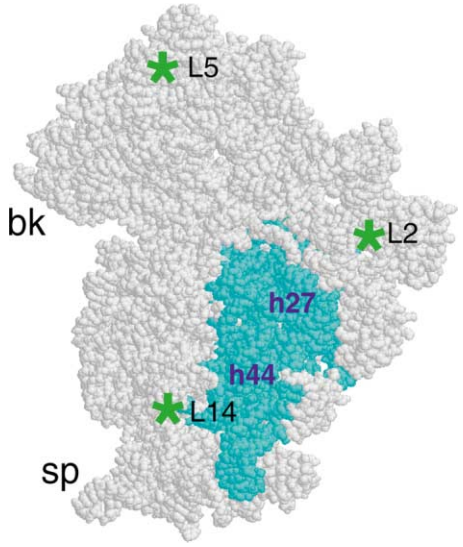

Figure 7. Diagrammatic Presentation of Interaction between the 30S Subunit and Proteins L2, L5, and L14

The interacting regions of L2, L5, and L14 on the 30S subunit are marked with stars. The geometrically rotational center region of the 30S subunit is colored in cyan. Landmarks: bk, beak; sp, spur.

The Role of Ribosomal Proteins

The importance of RNA in the translation process has been stressed since the functional core of the ribosome including the decoding center and the peptidyl-transferase center were observed to be rich in RNA in the crystal structures (Ban et al., 2000, Wimberly et al., 2000). Therefore, the role of the ribosomal proteins is now generally regarded as ancillary, mainly important for assembly of the complete 70S structure and for maintaining its stability (Ban et al., 2000; Moore and Steitz, 2002). In the analysis of the ratchet-like movement, we found that many ribosomal proteins participate directly and actively in the large conformational changes (Figure 6D), especially in important functional regions, such as the mRNA entrance and exit channel, polypeptide exit tunnel, and some of the inter-subunit bridges, in contrast to the low mobility of most of the RNA regions. From the initiation-like to the EF-G·GTP bound state, the opening up of the mRNA channel in the 30S subunit apparently facilitates the passing of the mRNA (Frank and Agrawal, 2000). An overall outward movement of the proteins in the 50S subunit is likely associated with the smaller compactness of the ribosome in the EF-G·GTP bound state.

Since the protein structure always has much more freedom than RNA, a possible explanation of the protein behaviors is that the large changes in the protein are induced by small changes in the RNA. One typical example is the switch of the residues 885 and 888 in helix 27 of 16S rRNA, which induces a large rearrangement of RNA and proteins (Gabashvili et al., 1999). While the RNA structure of the 50S subunit in most parts shows little change, especially in the central bridging regions, three proteins residing on the periphery near the inter-subunit surface, L2, L5, and L14, show considerable movement. Since these proteins are involved in bridge formation with the 30S subunit, it is conceivable that they have a pivotal role in modulating the ratchet-like movement of 30S subunit relative to the 50S subunit. Strikingly, a close check shows that all three proteins interact with functionally important RNA regions of the 50S subunit that display prominent movement. L2 is located near the base of the L1 stalk, and the observed movement of L2 from the initiation-like to the EF-G·GTP bound state is in concert with the large "swing" motion of the L1 stalk (helix 76) mentioned in the preceding section, implying that both movements are coupled. Protein L2 was proven to be functionally important in the peptidyl-transferase activity (Uhlein et al., 1998; Cooperman et al., 1995). Turning to L14, it is the only protein that interacts directly with the sarcin-ricin loop (SRL), which is in immediate vicinity to the GTPase-associated center. From the initiation-like to the EF-G·GTP bound state, L14 performs a 14 degree rotation while SRL moves by less than 3 Å, suggesting that the large movement of L14 is likely induced by the small changes of SRL. Similarly, L5 interacts directly with 5S rRNA, which is one of the RNA regions that undergo substantial changes during the ratchet-like motion. The large movement of L5 is therefore likely correlated with the changes in the 5S rRNA. More strikingly, a superimposition of the 30S subunit and the above three proteins reveals that these proteins lie close to the periphery of the 30S subunit and form a large triangle, whose center is close to the rotational center of the 30S subunit (Figure 7). Thus, the positions of L2, L5, and L14, and their considerable movements between the initiation-like and the EF-G·GTP bound states suggest that these proteins are optimally placed for modulating the rotation of the 30S subunit.

Experimental Procedures

Cryo-EM

The sample preparation, electron microscopy and image processing of the initiation-like complex were described in detail previously (Gabashvili et al., 2000). The 12.3 Å EF-G·GTP bound complex was obtained from a total of 50,854 projections of the EFG·GMPP(CH2)·

ribosome complex as described earlier (Agrawal et al., 1999a). The micrographs were recorded on a Philips FEI (Eindhoven, The Netherlands) Tecnai F20 field emission gun electron microscope at a magnification of 50,000 and at 200 kV with an electron dose of ~20e$^-$/Å^2. After a check for drift, astigmatism, and the presence of Thon rings, micrographs were scanned on a Zeiss-Imaging scanner (Z/I Imaging Corporation, Huntsville, AL) with a sampling step corresponding to a pixel size of 2.82 Å on the object scale. The complete 3D reconstruction was done in SPIDER (Frank et al, 1996) following standard procedures. The final resolution was determined by using the Fourier shell correlation curve with a 0.5 cut off.

Both volumes were amplitude-corrected by using low-angle X-ray scattering data. Prior to the application of the real-space refinement, the EF-G fragments in the GTP state volume were removed. The two volumes were brought to the same scale, by changing the pixel size of the initiation-like volume from 2.93 to 2.82 Å, and then aligned with each other.

RSRef and TNT

The molecule was placed into a unit cell of dimensions 366.6 × 366.6 × 366.6 Å, calculated from the dimension (130 × 130 × 130 pixels) and pixel size (2.82 Å) of the cryo-EM map. The high-resolution limits were set to the resolutions of the cryo-EM density maps. The low-resolution limit was set to 100 Å for both volumes. As an all-atom structure was used in the computation, over 120,000 atoms were included in the refinement. Additional parameters included: (1) a refinement cut off radius (3.5 Å), limiting the distance between atoms and grid points used for scaling and derivative calculation and (2) a calculation cut off radius (7.5 Å) beyond which the contribution of an atom to the electron density is assumed to be zero. Computations for the real-space refinement were done on an Origin 2000 (Silicon Graphics, Mountain View, CA).

After real-space refinement, fitted coordinates were subjected to few steps of energy minimization (Discover, Accelrys Inc.) to relieve unfavorable steric interactions, without deviating from the fitted backbone atomic positions.

Acknowledgments

We thank Michael Watters and Yu Chen for preparing the illustrations. This work was supported by NIH R37 GM 29169 (J.F.), NIH R01 GM 55440 (J.F.), NIH P01 GM 64676 (T.A. Cross/MSC), NSF DBI-98-08098 (M.S.C.), NIH R01 GM 54762 (A.S.), NIH P50 GM62529, Sun Academic Equipment Grant. EDUD-7824-020257-US (A.S.), NIH R01 GM 53827(SCH), and NIH R01 GM 61576 (R.K.A.).

Received: March 10, 2003
Revised: April 17, 2003
Accepted: May 8, 2003
Published: June 12, 2003

References

Agrawal, R.K., Penczek, P., Grassucci, R.A., and Frank, J. (1998). Visualization of elongation factor G on the Escherichia coli 70S ribosome: the mechanism of translocation. Proc. Natl. Acad. Sci. USA *95*, 6134–6138.

Agrawal, R.K., Heagle, A.B., Penczek, P., Grassucci, R.A., and Frank, J. (1999a). EF-G-dependent GTP hydrolysis induces translocation accompanied by large conformational changes in the 70S ribosome. Nat. Struct. Biol. *6*, 643–647.

Agrawal, R.K., Penczek, P., Grassucci, R.A., Burkhardt, N., Nierhaus, K.H., and Frank, J. (1999b). Effect of buffer conditions on the position of tRNA on the 70S ribosome as visualized by cryoelectron microscopy. J. Biol. Chem. *274*, 8723–8729.

Agrawal, R.K., Linde, J., Sengupta, J., Nierhaus, K.H., and Frank, J. (2001). Localization of L11 protein on the ribosome and elucidation of its involvement in EF-G-dependent translocation. J. Mol. Biol. *311*, 777–787.

Altschul, S.F., Madden, T.L., Schaffer, A.A., Zhang, J., Zhang, Z., Miller, W., and Lipman, D.J. (1997). Gapped BLAST and PSI-BLAST: a new generation of protein database search programs. Nucleic Acids Res. *25*, 3389–3402.

Ban, N., Nissen, P., Hansen, J., Moore, P.B., and Steitz, T.A. (2000). The complete atomic structure of the large ribosomal subunit at 2.4 Å resolution. Science *289*, 905–920.

Brodersen, D.E., Clemons, W.M., Carter, A.P., Wimberly, B.T., and Ramakrishnan, V. (2002). Crystal structure of the 30S ribosomal subunit from Thermus thermophilus: structure of the proteins and their interactions with 16S RNA. J. Mol. Biol. *316*, 725–768.

Carson, M. (1991). Ribbons 2.0. J. Appl. Crystallog. *24*, 958–961.

Cate, J.H., Yusupov, M.M., Yusupova, G.Z., Earnest, T.N., and Noller, H.F. (1999). X-ray crystal structures of 70S ribosome functional complexes. Science *285*, 2095–2104.

Chapman, M.S. (1995). Restrained real-space macromolecular atomic refinement using a new resolution-dependent electron density function. Acta Crystallogr. *A51*, 69–80.

Chen, L.F., Blanc, E., Chapman, M.S., and Taylor, K.A. (2001). Real space refinement of acto-myosin structure from sectioned muscle. J. Struct. Biol. *133*, 221–232.

Cooperman, B.S., Wooten, T., Romero, D.P., and Traut, R.R. (1995). Histidine 229 in protein L2 is apparently essential for 50S peptidyl transferase activity. Biochem. Cell Biol. *73*, 1087–1094.

Frank, J., Verschoor, A., Li, Y., Zhu, J., Lata, R.K., Radermacher, M., Penczek, P., Grassucci, R., Agrawal, R.K., and Srivastava, S. (1995a). A model of the translational apparatus based on a three-dimensional reconstruction of the Escherichia coli ribosome. Biochem. Cell Biol. *73*, 757–765.

Frank, J., Zhu, J., Penczek, P., Li, Y., Srivastava, S., Verschoor, A., Radermacher, M., Grassucci, R., Lata, R.K., and Agrawal, R.K. (1995b). A model of protein synthesis based on cryo-electron microscopy of the E. coli ribosome. Nature *376*, 441–444.

Frank, J. (1996). Three-Dimensional Electron Microscopy of Macromolecular Assemblies (San Diego, CA: Academic Press).

Frank, J., Radermacher, M., Penczek, P., Zhu, J., Li, Y., Ladjadj, M., and Leith, A. (1996). SPIDER and WEB: processing and visualization of images in 3D electron microscopy and related fields. J. Struct. Biol. *116*, 190–199.

Frank, J., and Agrawal, R.K. (2000). A ratchet-like inter-subunit reorganization of the ribosome during translocation. Nature *406*, 318–322.

Frank, J., and Agrawal, R.K. (2001). Ratchet-like movements between the two ribosomal subunits: their implications in elongation factor recognition and tRNA translocation. Cold Spring Harbor Symposia on Quantitative Biology. (Cold Spring, NY: Cold Spring Harbor Laboratory Press), pp. 67–75.

Frank, J., Penczek, P., Grassucci, R.A., Heagle, A.B., Spahn, C.M.T., and Agrawal, R.K. (2000). Cryo-electron microscopy of the translational apparatus: experimental evidence for the paths of mRNA, tRNA, and the polypeptide chain. In The Ribosome: Structure, Function, Antibiotics and Cellular Interactions, R.A. Garrett, S.R. Douthwaite, A. Liljas, A.T. Matheson, P.B. Moore, and H.F. Noller, eds. (Washington, D.C.: ASM Press), pp. 45–51.

Gabashvili, I.S., Agrawal, R., Grassucci, R., Squires, C.L., Dahlberg, A.E., and Frank, J. (1999). Major rearrangements in the 70S ribosomal 3D structure caused by a conformational switch in 16S ribosomal RNA. EMBO J. *18*, 6501–6507.

Gabashvili, I.S., Agrawal, R.K., Spahn, C.M.T., Grassucci, R.A., Svergun, D.I., Frank, J., and Penczek, P. (2000). Solution structure of the E. coli 70S ribosome at 11.5 Å resolution. Cell *100*, 537–549.

Gabashvili, I.S., Gregory, S.T., Valle, M., Grassucci, R., Worbs, M., Wahl, M.C., Dahlberg, A.E., and Frank, J. (2001). The polypeptide tunnel system in the ribosome and its gating in erythromycin resistance mutants of L4 and L22. Mol. Cell *8*, 181–188.

Gomez-Lorenzo, M.G., Spahn, C.M.T., Agrawal, R.K., Grassucci, R.A., Penczek, P., Chakraburtty, K., Ballesta, J.P., Lavandera, J.L., Garcia-Bustos, J.F., and Frank, J. (2000). Three-dimensional cryo-electron microscopy localization of EF2 in the Saccharomyces cerevisiae 80S ribosome at 17.5 Å resolution. EMBO J. *19*, 2710–2718.

Harms, J., Schluenzen, F., Zarivach, R., Bashan, A., Gat, S., Agmon,

I., Bartels, H., Franceschi, F., and Yonath, A. (2001). High resolution structure of the large ribosomal subunit from a mesophilic eubacterium. Cell *107*, 679–688.

Jones, T.A., Zou, J.Y., Cowan, S.W., and Kjeldgaard, M. (1991). Improved methods for building protein models in electron density maps and the location of errors in these models. Acta Crystallogr. *A47*, 110–119.

Laughrea, M., and Moore, P.B. (1977). Physical properties of ribosomal protein S1 and its interaction with the 30S ribosomal subunit of Escherichia coli. J. Mol. Biol. *112*, 399–421.

Malhotra, A., Penczek, P., Agrawal, R.K., Gabashvili, I.S., Grassucci, R.A., Junemann, R., Burkhardt, N., Nierhaus, K.H., and Frank, J. (1998). Escherichia coli 70 S ribosome at 15 Å resolution by cryo-electron microscopy: localization of fMet-tRNAfMet and fitting of L1 protein. J. Mol. Biol. *280*, 103–116.

Martí-Renom, M.A., Stuart, A.C., Fiser, A., Sanchez, R., Melo, F., and Sali, A. (2000). Comparative protein structure modeling of genes and genomes. Annu. Rev. Biophys. Biomol. Struct. *29*, 291–325.

Moore, P.B., and Steitz, T.A. (2002). The involvement of RNA in ribosome function. Nature *418*, 229–235.

Nissen, P., Hansen, J., Ban, N., Moore, P.B., and Steitz, T.A. (2000). The structural basis of ribosome activity in peptide bond synthesis. Science *289*, 920–930.

Ogle, J.M., Brodersen, D.E., Clemons, W.M., Jr., Tarry, M.J., Carter, A.P., and Ramakrishnan, V. (2001). Recognition of cognate transfer RNA by the 30S ribosomal subunit. Science *292*, 897–902.

Pieper, U., Eswar, N., Stuart, A.C., Ilyin, V.A., and Sali, A. (2002). MODBASE, a database of annotated comparative protein structure models. Nucleic Acids Res. *30*, 255–259.

Roseman, A.M. (2000). Docking structures of domains into maps from cryo-electron microscopy using local correlation. Acta Crystallogr. *D56*, 1332–1340.

Rossmann, M.G. (2000). Fitting atomic models into electron-microscopy maps. Acta Crystallogr. *D56*, 1341–1349.

Sali, A., and Blundell, T.L. (1993). Comparative protein modeling by satisfaction of spatial restraints. J. Mol. Biol. *234*, 779–815.

Sanchez, R., and Sali, A. (1998). Large-scale protein structure modeling of the Saccharomyces cerevisiae genome. Proc. Natl. Acad. Sci. USA *95*, 13597–13602.

Schaffer, A.A., Wolf, Y.I., Ponting, C.P., Koonin, E.V., Aravind, L., and Altschul, S.F. (1999). IMPALA: matching a protein sequence against a collection of PSI-BLAST-constructed position-specific score matrices. Bioinformatics *15*, 1000–1011.

Schluenzen, F., Tocilj, A., Zarivach, R., Harms, J., Gluehmann, M., Janell, D., Bashan, A., Bartels, H., Agmon, I., Franceschi, F., and Yonath, A. (2000). Structure of functionally activated small ribosomal subunit at 3.3 Å resolution. Cell *102*, 615–623.

Sengupta, J., Agrawal, R.K., and Frank, J. (2001). Visualization of protein S1 within the 30S ribosomal subunit and its interaction with messenger RNA. Proc. Natl. Acad. Sci. USA *98*, 11991–11996.

Serdyuk, I., Baranov, V., Tsalkova, T., Gulyamova, D., Pavlov, M., Spirin, A., and May, R. (1992). Structural dynamics of translating ribosomes. Biochimie *74*, 299–306.

Spahn, C.M.T., Beckmann, R., Eswar, N., Penczek, P.A., Sali, A., Blobel, G., and Frank, J. (2001). Structure of the 80S ribosome from *Saccharomyces cerevisiae*--tRNA-ribosome and subunit-subunit interactions. Cell *107*, 373–386.

Stark, H., Rodnina, M.V., Wieden, H.J., Zemlin, F., Wintermeyer, W., and van Heel, M. (2002). Ribosome interactions of aminoacyl-tRNA and elongation factor Tu in the codon-recognition complex. Nat. Struct. Biol. *9*, 849–854.

Tronrud, D.E., Ten Eyck, L.F., and Matthews, B.W. (1987). An efficient general-purpose least-squares refinement program for macromolecular structures. Acta Crystallogr. *A43*, 489–501.

Tung, C.S., Joseph, S., and Sanbonmatsu, K.Y. (2002). All-atom homology model of the Escherichia coli 30S ribosomal subunit. Nat. Struct. Biol. *9*, 750–755.

Uhlein, M., Weglohner, W., Urlaub, H., and Wittmann-Liebold, B. (1998). Functional implications of ribosomal protein L2 in protein biosynthesis as shown by in vivo replacement studies. Biochem. J. *331*, 423–430.

Valle, M., Sengupta, J., Swami, N.K., Grassucci, R.A., Burkhardt, N., Nierhaus, K.H., Agrawal, R.K., and Frank, J. (2002). Cryo-EM reveals an active role for aminoacyl-tRNA in the accommodation process. EMBO J. *21*, 3557–3567.

Volkmann, N., and Hanein, D. (1999). Quantitative fitting of atomic models into observed densities derived by electron microscopy. J. Struct. Biol. *125*, 176–184.

Wimberly, B.T., Brodersen, D.E., Clemons, W.M., Morgan-Warren, R.J., Carter, A.P., Vonrhein, C., Hartsch, T., and Ramakrishnan, V. (2000). Structure of the 30S ribosomal subunit. Nature *407*, 327–339.

Wriggers, W., and Birmanns, S. (2001). Using Situs for flexible and rigid-body fitting of multi resolution single-molecule data. J. Struct. Biol. *133*, 193–202.

Yusupov, M.M., Yusupova, G.Z., Baucom, A., Lieberman, K., Earnest, T.N., Cate, J.H., and Noller, H.F. (2001). Crystal structure of the ribosome at 5.5 Å resolution. Science *292*, 883–896.

Yusupova, G.Z., Yusupov, M.M., Cate, J.H., and Noller, H.F. (2001). The path of messenger RNA through the ribosome. Cell *106*, 233–241.

Accession Numbers

Atomic models have been deposited in the Protein Data Bank under the following ID codes: 1P6G (30S, EF-G·GTP bound state); 1P85 (50S, EF-G·GTP bound state); 1P87 (30S, initiation-like state); and 1P86 (50S, initiation-like state).